Inorganic Chemistry
Article
pubs.acs.org/IC

Revisited: Decomposition or Melting? Formation Mechanism Investigation of $LiCoO_2$ via In-Situ Time-Resolved X-ray Diffraction

Scott A. Wicker and Edwin H. Walker, Jr.*

Department of Chemistry, Southern University and A & M College, Baton Rouge, Louisiana 70813, United States

ABSTRACT: We report the first in-situ time-resolved X-ray diffraction investigation in conjunction with a non-isothermal kinetic study using the model-free isoconversional kinetic method to determine the formation mechanism for the solid-state synthesis of electrochemically active $LiCoO_2$ from Li_2CO_3 and Co_3O_4. Detailed information on the phase evolution as well as thermal events during the heating process was clearly observed, explained, and supported. This investigation provides structural as well as kinetic evidence for a multistep reaction and proposes the first plausible formation mechanism for the solid-state synthesis of $LiCoO_2$.

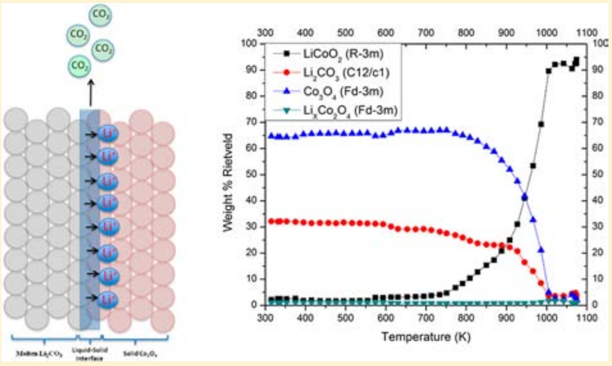

INTRODUCTION

For decades, conventional thought has supported the idea that metal−organic precursor based (e.g. sol−gel and/or Pechini process) synthesis processes proceed via the self-propagating combustion of the metal−organic precursors. While the organic moieties behave as fuels, the reaction mechanism is propelled forward, which results in the production of the desired ternary metal oxides. Combustion reactions are understood to obey a mechanism in which the metal−organic precursors first decompose into metal carbonates. As the reaction continues, the metal carbonates decompose into metal oxides. There is some validity to this way of thinking; however, the nature of the combustion reaction must be revisited. Consider the following: it is largely accepted that a metal carbonate is the most probable product in the decomposition of metal organic precursors below 400 °C. As well, it is well documented throughout various literature sources that metal carbonates decompose at very high temperatures, usually in excess of 1500 °C. However, phase pure ternary metal oxides are produced in the majority of metal−organic precursor based synthesis methods well below the decomposition temperature of the respective metal carbonates. These considerations raise questions about the understanding of reaction mechanisms.

Although ternary metal oxides can be synthesized by various processes, physical properties such as the electrochemical performance of the material depend on many factors such as phase composition, particle size/distribution, and crystallinity.[1] For example, $LiCoO_2$ has been chosen as one of the prime cathode materials for secondary lithium ion batteries due to its high specific capacity and energy density, excellent cycle life, and ease of synthesis.[2] However, a general solid-state method, which involves a solid-state reaction between Li_2CO_3 and Co_3O_4, is employed to produce the desired electrochemically active crystalline phase.[2−6] This solid-state method uses the thermal treatment of reagents in either a non-isothermal and/or isothermal environment at elevated temperatures (~1073.15 K). Researchers also have performed the solid-state synthesis of $LiCoO_2$ at low temperatures; however the material produced with this technique is not electrochemically favored.[7−9] $LiCoO_2$ can exist in either a rhombohedral or cubic crystal structure. These structures are based on the same oxide sublattice; however, they are distinguished by the spatial arrangement of divalent and trivalent cations as well as the distance along the c axis and the angle γ.[7−10] In order to achieve the preferred highly electrochemically active structure, $LiCoO_2$ must have a rhombohedral symmetry with an $R\bar{3}m$ space group in which lithium ions and cobalt ions are situated in 3a and 3b sites and oxygen ions in 6c sites. In the $R\bar{3}m$ structure of $LiCoO_2$, 3a and 3b sites are equivalent to the oxygen ion close packed cubic octahedral sites. With these sites occupied, a hexagonal close packed layered framework is constructed. The layered structure of $LiCoO_2$ provides a two-dimensional route for electrochemical lithium intercalation and de-intercalation into the 3a sites.

To date, the solid-state methods are predominantly adopted in industry for mass production due to their low cost and ease of implementation. Despite the numerous studies of $LiCoO_2$, the reaction kinetics of the formation of $LiCoO_2$ and pure in-situ structural analysis during solid-state reactions between Li_2CO_3 and Co_3O_4 have never been examined in detail until now.

This report describes the first non-isothermal investigation of the dependence of the activation energy (E_α) on the extent of conversion (α) of $LiCoO_2$ using the iso-conversional method of Friedman in conjunction with an in-situ time-resolved X-ray

Received: July 12, 2012
Published: January 31, 2013

dx.doi.org/10.1021/ic301516a | *Inorg. Chem.* 2013, 52, 1772−1779

diffraction study to determine a plausible formation mechanism for electrochemically active $LiCoO_2$. The knowledge of the reaction complexity for the formation of the $LiCoO_2$ is instrumental in the optimization of the synthesis conditions that are required for the formation of particles with uniform particle size and distribution.

■ THEORETICAL BACKGROUND

Isothermal as well as non-isothermal methods have been used extensively for the analysis of solid-state kinetics. Traditionally, kinetic analysis of solid-state reactions is usually based on a single step kinetic eq 1

$$\frac{d\alpha}{dt} = k(t)f(\alpha) \tag{1}$$

where t is the time, T is the temperature, α is the extent of conversion, and $f(\alpha)$ is the reaction model. The degree of conversion (α) of the process is expressed as

$$\alpha = \frac{m_0 - m_T}{m_0 - m_f} \tag{2}$$

where m_0 is the initial mass, m_T is the mass at a specified temperature, and m_f is the final mass.[11]

The reaction model may take various forms, some of which are shown in Table 1. The explicit temperature dependence of the rate constant is introduced by replacing $k(T)$ with the Arrhenius equation, which gives

Table 1. Set of Alternate Reaction Models Applied To Describe the Thermal Transformations in Solids

	reaction model	$f(\alpha)$
1	Power Law	$4\alpha^{3/4}$
2	Power Law	$3\alpha^{2/3}$
3	Power Law	$2\alpha^{1/2}$
4	Power Law	$2/3\alpha^{-1/2}$
5	one-dimensional diffusion	$1/2\alpha^{-1}$
6	Mampel (first order)	$1 - \alpha$
7	Avrami–Erofeev	$4(1 - \alpha)[-\ln(1 - \alpha)^{3/4}$
8	Avrami–Erofeev	$3(1 - \alpha)[-\ln(1 - \alpha)^{2/3}$
9	Avrami–Erofeev	$2(1 - \alpha)[-\ln(1 - \alpha)^{1/2}$
10	three-dimensional diffusion	$2(1 - \alpha)^{2/3}(1 - (1 - \alpha)^{1/3})^{-1}$
11	contracting sphere	$3(1 - \alpha)^{2/3}$
12	contracting cylinder	$2(1 - \alpha)^{1/2}$

$$\frac{d\alpha}{dt} = A\exp\left(\frac{-E}{RT}\right)f(\alpha) \tag{3}$$

where A (the pre-exponential factor) and E (the activation energy) are the Arrhenius parameters and R is the gas constant. The Arrhenius parameters, together with the reaction model, are sometimes called the kinetic triplet. Under non-isothermal conditions in which a sample is heated at a constant rate, the explicit temporal dependence in eq 2 is eliminated through the trivial transformation

$$\frac{d\alpha}{dt} = \frac{A}{\beta}\exp\left(\frac{-E}{RT}\right)f(\alpha) \tag{4}$$

where $\beta = dT/dt$ is the heating rate.

Often the Arrhenius parameters obtained from non-isothermal data are reported to disagree with the values derived from isothermal experiments. Vyazovkin et al. offers two major reasons for this discrepancy. The widespread use of kinetic methods that involve force fitting of non-isothermal data to hypothetical reaction models is the primary basis for the discrepancy. If one follows this model-fitting approach, the Arrhenius parameters are determined by the assuming function $f(\alpha)$. Since T as well as α varies simultaneously in the non-isothermal experiment, the model-fitting approach in general fails to cleanly separate from the temperature dependence, $k(T)$, and the reaction model, $f(\alpha)$.[12] As a consequence, practically any $f(\alpha)$ can satisfactorily fit the data at the expense of drastically varying the Arrhenius parameters, which compensate for the difference between the assumed function of $f(\alpha)$ and the true but unknown reaction model. For this reason, the model-fitting methods tend to produce highly uncertain values of Arrhenius parameters.

Isothermal and non-isothermal experiments are inevitably conducted in different temperature regions, which results in another major reason for the discrepancy in values. If the solid-state reaction involves several steps with different activation energies, the contribution of these steps to the overall decomposition rate measured in a thermal analysis experiment will differ with both temperature and extent of conversion. Therefore, the effective activation energy determined from thermal analysis experiments will also be a function of temperature and percent conversion. The primus of the model-fitting methods is targeted toward obtaining a single value of the activation energy for an overall process. The values extracted using model-fitting methods is in fact an average that reflects changes in the reaction mechanism and kinetics with the temperature and the extent of conversion. However, the model-free isoconversional method allows for unmistakably detecting multistep kinetics as a dependence of the activation energy on the extent of conversion. Furthermore, it was shown[13] that revealing the dependence of the activation energy on conversion not only helps to disclose the complexity of a process but also helps identify its kinetic scheme. The shapes of the dependence of E_α on α have been identified from simulated data for competing,[13] independent,[14] consecutive[15] and reversible reactions,[16] as well as reactions complicated by diffusion.[17]

Isoconversional methods or the Friedman method,[18−20] which is named after the researcher who first derived the method, are capable of addressing the shortcomings of the model-fitting methods. These methods allow the activation energy to be determined as a function of the extent of conversion and/or temperature. As well, this dependence is determined without making assumptions about the reaction model. Since the model-free isoconversional methods eliminate the causes of the discrepancies, they are likely to produce consistent kinetic results from isothermal and non-isothermal experiments. Thus, if a range of linear heating experiments at different heating rates, β, are performed and the times at which a percent conversion is achieved can be identified for each linear heating experiment, $f(\alpha)$ will be a constant. By measuring T and $d\alpha/dt$ at that percent conversion for each of the experiments, we can obtain E from the slope of plots of ln $d\alpha/dt$ versus $1/T$. However, $d\alpha/dt$ can be difficult to measure accurately. Since the heating rate is much easier to determine accurately, one usually prefers to rewrite the latter equation to

$$\ln\left(\frac{d\alpha}{dT}\beta\right) = -\frac{E}{RT} - \ln f(\alpha) \tag{5}$$

The activation energy, E, is now determined from the slope of plots of $\ln((d\alpha)/(dt)\beta)$ versus $1/T$. The method does not require any assumption on $f(\alpha)$; therefore, it is a so-called model-free method.

■ EXPERIMENTAL AND INSTRUMENTAL

In this study, the transmission of monochromatic high-intensity X-rays was used for in-situ monitoring of the phase changes during the reaction. As well, thermogravimetric analysis (TGA) was used to record the thermal events of the process. The in-situ X-ray measurement was performed using a nonambient X-ray scattering technique[21,22] coupled with a Mar 345 image plate detector. The experiment was carried out at the X-ray Operations and Research Beamline 1-BM-C at the Advanced Photon Source of Argonne National Laboratory.[22] Nearly stoichiometric amounts of Li_2CO_3 and Co_3O_4 (with about 3% lithium (mol) in excess) were mixed and inserted into a fused silica capillary. (Lithium carbonate and cobalt (II, III) oxide were purchased from Aldrich Chemicals.) The capillary was heated at a heating rate of 10 K min^{-1} under an oxygen atmosphere from 323.15 to 1073.15 K. Two dimensional powder X-ray diffraction (XRD) pattern of the reaction mixture was recorded every 2 min using wavelength $\lambda = 0.6066$ Å at an oscillation width and time of 7° and 3.5 s, respectively. All diffraction peaks were identified and the data were fit to $R_{wp} < 10$ using the TOPAS Rietveld refinement software package. Empirical parameters where determine from LaB_6 measurements using the Pseudo-Voigt (PV-TCHZ) method. The U, V, W, and X parameters were 0.08293955, −0.02397586, 0.01075575, and 0.01410234, respectively. These parameters were fixed for all subsequent experiments to ensure that any change in peak profile was observed. This experimental setup affords a thorough monitoring of the structural evolution of phase pure rhombohedral ($R\bar{3}m$) $LiCoO_2$ from the monoclinic ($C12/c1$) Li_2CO_3, and the spinel ($Fd\bar{3}m$) Co_3O_4.

■ RESULTS AND DISCUSSION

Non-Isothermal Investigation Results. The activation energies at various percent conversions associated with the solid-state reaction of Li_2CO_3 and Co_2O_3 were determined using the Friedman model-free method.[16,19,23,24] The non-isothermal kinetic experiments were performed under an air atmosphere using a simultaneous TGA/DTA (SDT) (Q600, TA Instruments). The temperature and energy of the SDT were calibrated by standard pure indium. To ensure the accuracy of quantitative analytical results of the SDT, samples of the $LiCoO_2$ starting material were pressed into pellets that ranged from 3 to 5 mg, which is in accordance with American Society for Testing and Materials (ASTM) procedure E1641. The six different heating rates, β, chosen for the non-isothermal kinetic investigation were 1, 5, 10, 20, 30, and 40 K/min as shown in Figure 1.

The temperature at which the fraction of conversion, α, was reached at heating rate, β, from room temperature until 1073.15 K as shown in Table 2. High correlation coefficients ($r^2 > 0.98$) were acquired for all of the linear regression curves of $\ln[\beta]$ vs $1/T_\alpha$, and the slopes at each conversion were used to calculate the plot of the activation energies vs fraction of conversion in Figure 2.

The slope of the plot $\ln[\beta(d\alpha/dt)]$ vs $1/T_\alpha$ gives the value of the activation energy related to a given conversion. The values of activation energies (E_a) of the investigated solid-state reaction of Li_2CO_3 and Co_3O_4 at different constant values of α, which were determined by Friedman (FR) method, are shown in Table 3. The mean value ($\bar{X}$) of the activation energy determined using Friedman model-free method was 251 kJ mol^{-1}.

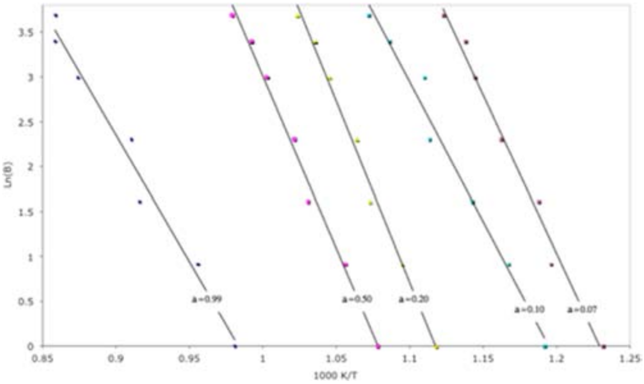

Figure 1. This is a composite of the data in Table 2 plotted as $\ln[\beta]$ vs $1/T_\alpha$ for α = 0.07, 0.10, 0.20, 0.50, and 0.90.

Table 2. The Extrapolated Temperature (in K) at which the Fraction of Conversion was Reached at Heating Rate

β (K min^{-1})	T_α (0.07)	T_α (0.10)	T_α (0.20)	T_α (0.50)	T_α (1.0)
1.0	804	812	822	831	839
5.0	830	842	853	864	875
10.0	847	861	874	885	895
20.0	861	874	876	887	901
30.0	862	879	893	907	921
40.0	876	891	905	920	933

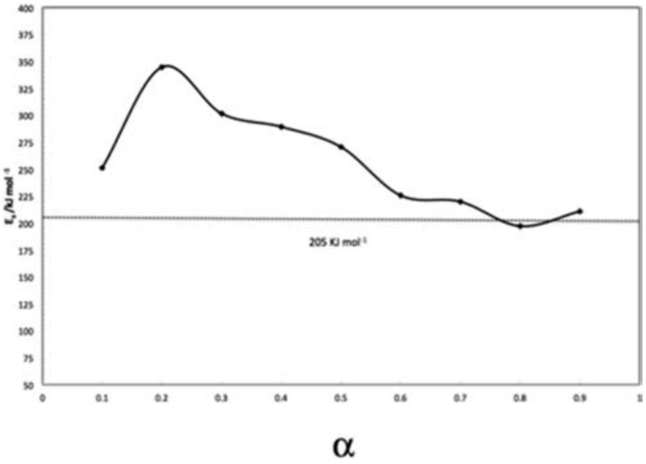

Figure 2. Dependencies of the activation energy on extent of conversion determined using the model-free isoconversional technique for the non-isothermal data.

Table 3. Activation Energies at Various Percent Conversions

α	E_a (Friedman method) in kJ mol^{-1}	E_a (Flynn-Wall) in kJ mol^{-1}
0.1	251	243
0.2	344	320
0.3	301	327
0.4	289	315
0.5	270	302
0.6	225	284
0.7	219	231
0.8	197	220
0.9	210	208

Figure 2 shows the dependence of the activation energy on the $LiCoO_2$ conversion, as computed by the isoconversional method. When all six data sets are included in the analysis, the activation energy increases to maximum of 344 kJ/mol at 20% conversion, then decreases gradually to 197 kJ/mol at 80% conversion, and increases slightly to 210 kJ/mol near the end of the reaction. Unlike the model fitting method, which yields a single overall value of activation energy for the process (the dotted line that indicates a global activation energy of 205 kJ/mol for the formation of $LiCoO_2$), the isoconversional technique reveals complexity of the reaction mechanism in the form of a functional dependence of the activation energy on the extent of conversion.

Because most solid-state reactions are not simple one-step processes, analysis of non-isothermal data by the isoconversional technique is well suited for revealing this type of complexity that is disguised in the model fitting kinetic analysis. It has been demonstrated[18] that the isoconversional method applied to a multistep process reveals the dependence of E_α on α. Subsequently, it was shown[13] that this dependence helps not only to disclose the complexity of a process but also to identify its kinetic scheme as well. The shapes of the dependence of E_α on α have been identified from model data for competing,[13] independent,[14] consecutive,[15] reversible reactions,[16] as well as for reactions complicated by diffusion.[17] The most characteristic dependencies are well documented.[16] Although the shape of the dependence of E_α on α does not necessarily explicitly identify the kinetic scheme of a process, it in all instances sheds light on the latter.

The variation in activation energy with conversion of solid-state reaction of Li_2CO_3 and Co_3O_4 suggests the possibility of consecutive or simultaneous thermal events. This behavior may be indicative of a multistep reaction mechanism in which an early step in the mechanism having a high activation energy can dominate the kinetics at faster heating due to the higher temperatures reached in that type of experiment.

In the temperature range of 700−900 K, the increased dependence of the E_α on α corresponds to the agglomeration of Li_2CO_3 particles that hinders the diffusion and release of the CO_2 gas.[25] Once Li_2CO_3 begins to melt, there is a decreased dependence of E_α on α that corresponds to the liberation of CO_2 gas, which indicates an endothermic reaction followed by an irreversible reaction as shown in Figure 3.[16] Finally, the increased dependence E_α on α near the end of the reaction can be attributed to the diffusion of lithium ions to the available octahedral sites followed by the structural rearrangement from cubic to rhombohedral.

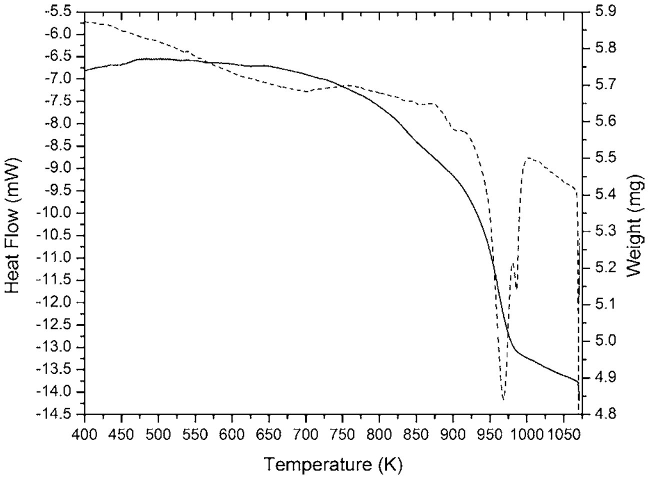

Figure 3. The TGA/DTA spectra of the solid-state reaction of Li_2CO_3 and Co_3O_4 at 10°/min.

When we analyze the TGA spectra that was performed 10° per minute, the spectra reveals three major weight losses in the heating process, which are in the temperature range of 700−900 K, 900−1000 K, and 1000−1100 K, respectively (Figure 3). **Note:** The TGA spectrum performed at 10 per minute was selected because it has identical experimental parameters as the in-situ time-resolved XRD study that will follow this discussion. As well, the TGA spectra at 10 per minute has perfect agreement with the TGA experiments conducted at 1, 5, 20, 30, and 40° K/min respectively as shown in Figure 1. As expected, each TGA spectra experiences a shift to the right as the heating rate is increased as shown in Table 2. An initial 3% mass loss was observed in TGA of the $LiCoO_2$ precursor in the temperature range of 700−900 K. Although the decomposition of Li_2CO_3 appears to be simple, the process is rich with complications. It is apparent that CO_2 is released in the thermal decomposition of Li_2CO_3, which is a diffusive process by nature. However, the diffusion and release of the CO_2 gas is hindered by the agglomeration of Li_2CO_3 particles upon reaching the melting point as well as the low pressure of CO_2 saturated vapor (∼4 Torr at 1000 K).[25] As result, this explains the slow reaction rate in the temperature range of 700−900 K. Additionally, the unwillingness of lithium carbonate to melt corresponds to the increased dependence of the E_α on α, which is demonstrated by activation energy increases to maximum of 344 kJ/mol at 20% conversion in Figure 2. This is in agreement with the slow loss of Li_2CO_3 intensity as it reacts to form a ternary Li−Co−O compound as shown in Figure 4. The initial mass loss is followed by a 8% mass loss that occurs in the temperature range 900−1000 K, which is the region where Li_2CO_3 melts. As well, there are two endothermic events that are observed in this region in the DTA curve. In this temperature range, there are simultaneous thermal events taking place: two endothermic events that mask an exothermic thermal event. Evidence that an exothermic event has occurred and formation of target material can be seen in the in-situ XRD study as early as scan 30 (888.15 K). The first endothermic event in the region of 900−975 K is a result of Li_2CO_3 melting, and the second endothermic event in the region of 975−990 K is a result of the liberation of CO_2. Once Li_2CO_3 becomes molten, it functions as a flux that surrounds the Co_3O_4 particles.

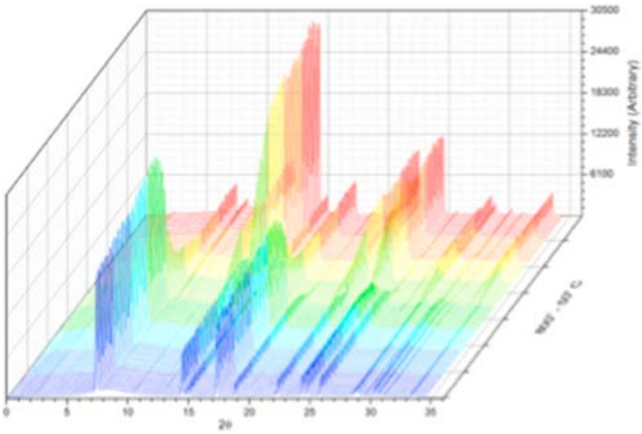

Figure 4. Time-resolved 2D-X-ray diffraction pattern of the solid-state reaction of Li_2CO_3 and Co_3O_4.

Historically, lithium salt fluxes have been used to encourage crystal growth. As well, there is a noticeable reaction rate increase accompanied by the liberation of CO_2 as shown in Figure 3. This endothermic event that is observed in both Figures 2 and 3 is indicative of a reversible reaction followed by an irreversible reaction. According to the literature, lithium carbonate decomposes above 1580 K, so the liberation of CO_2 in this region corresponds to the liquid−solid surface reaction in which Li^+ ions diffuse into the Co_3O_4 particle at the liquid−solid interface. During the final step, there is a 6% mass loss in temperature range of 1000−1100 K, as well as there are simultaneous thermal events taking place. These thermal events consist of the migration of both lithium and cobalt ions to the available octahedral sites, which proceeds at a moderate reaction rate. Evidence for the formation of the target material can be seen in the in-situ XRD pattern (Figure 4).

When there is an increasing dependence of E_α on α, this is indicative of a competing reaction.[13] However, some independent[14] and consecutive[15] reactions may also give rise to such a dependence. A decreasing dependence of E_α on α corresponds to the kinetic scheme of an endothermic reversible reaction followed by an irreversible reaction.[16] E_α is limited by the sum of the activation energy of the irreversible reaction and the enthalpy of the reversible reaction at low conversions and by the activation energy of the irreversible reaction at high conversions.

In-situ Time-Resolved XRD Investigation Results. The X-ray diffraction patterns were (Cu K_α) collected in 2 min intervals while heating the sample at 10 deg per minute from 323 to 1073 K in the range of 0−34 2θ at the Argonne Photon Source Beamline 1-BM-C with λ = 0.6066 Å, which corresponds to 0−120 2θ (Cu K_α). A total of 73 individual patterns were collected and analyzed. Quantitative Rietveld refinement calculations performed on all 73 patterns to determine the weight percent of Li_2CO_3 ($C12/c1$), Co_3O_4 ($Fd\bar{3}m$ and the plot of blue triangles in Figure 5), $LiCo_2O_4$ ($Fd\bar{3}m$ and the plot of green inverted triangles in Figure 5), and $LiCoO_2$ ($R\bar{3}m$) in each pattern (Figure 5). The waterfall plot of the X-ray diffraction patterns shows the presence of the two pure starting materials at ambient temperature (Figure 4). The high intensities observed for the diffraction of Co_3O_4 is due primarily to the high symmetry of the cubic phase and the Z number of cobalt within the spinel crystal lattice. The diffraction intensities of Li_2CO_3 are much weaker because of the lower Z number of lithium, carbon, and oxygen as well as the lower symmetry of the monoclinic crystal lattice. Above ambient temperature, all diffraction lines are shifted to lower 2θ due to the thermal expansion of the lattice planes of both the monoclinic and cubic crystalline phases. Upon heating to 850 K (scan 30), the diffraction intensity of Li_2CO_3 starts to decrease. When the temperature reaches approximate 850 K (scan 30), the diffraction peaks of $LiCoO_2$ start to form. Above this temperature, the crystallinity of $LiCoO_2$ increases further upon heating, while the diffraction peaks of Li_2CO_3 and Co_3O_4 gradually disappear. Neither the presence nor the formation of Li_2O or CoO was ever detected throughout this investigation.

When the weight percent as determined by Rietveld refinement is plotted versus temperature, the gradual rate of disappearance of Co_3O_4 (blue triangle) and appearance $LiCoO_2$ (black square) in the temperature range of 700−900 K is clearly shown in Figure 5. As well, the plots clearly demonstrate that the amount of Li_2CO_3 remains consistent in the temperature range of 300−700 K. However, there is a slow rate of disappearance of Li_2CO_3 in the temperature range of 700−900 K, which corresponds to the process of Li_2CO_3 forming agglomerate and then melting. Once Li_2CO_3 has completely melted, there is an increased rate of disappearance of Li_2CO_3 in the temperature range of 900−1000 K, which corresponds to the reaction at the solid−liquid interface that results in the release of CO_2.

In the temperature range of 900−1000 K, the reaction can best be described using Fick's Second Law of Diffusion. Essentially, there is a concentration gradient formed between the molten Li_2CO_3 and the solid Co_3O_4. At the concentration gradient or solid−liquid interface, Li ions diffuse into the area of lower concentration, the Co_3O_4. Li ions continue to diffuse until equilibrium, which is the formation of $LiCoO_2$, is achieved, and the diffusion of Li ions cease. Additionally, the unwillingness of lithium carbonate to melt is observed in the increased dependence of the E_α on α, which shown in Figure 2. This is in agreement with the slow loss of Li_2CO_3 intensity as it reacts to form a ternary Li−Co−O compound as shown in Figure 6. As well, the weight percentage confirms that there is an increase in the rate of formation of a lithiated cobalt oxide like $Li_2Co_2O_4$ and $LiCoO_2$ that is directly proportional to the rate of disappearance of Co_3O_4.

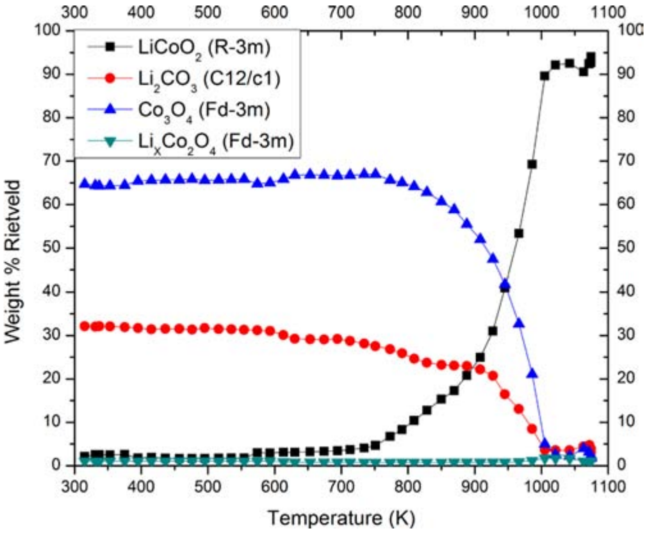

Figure 5. The plot of the weight percent of Li_2CO_3, $LiCoO_2$, and Co_3O_4 determined by Rietveld refinement in the solid-state reaction at 10°/min.

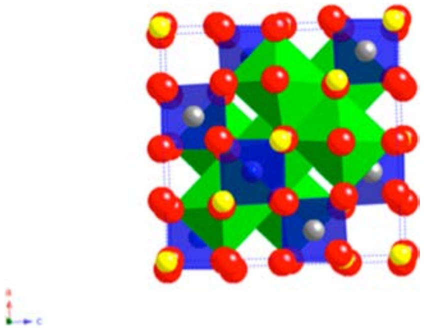

Figure 6. Intermediate formed between Scan 30−40 $Li_{2.5}Co_{2.5}O_4$ − $Fm\bar{3}m$ $Li_{0.5}$(8a) gray and Li_2 (16c) yellow, $Co^{2+}{}_{0.5}$(8a) blue, $Co_2{}^{3+}$(16d) green, O_4(32e) red.

Due to the high melting temperature of Co_3O_4 (~1168 K), it remains in the solid phase. The molten Li_2CO_3 surrounds the Co_3O_4 particles and then proceeds to react with Co_3O_4 at the liquid solid interface. The Li^+ ions are then available to diffuse into the available 8a, empty 8b tetrahedral sites, and empty 16c octahedral sites the of Co_3O_4 lattice. As lithium diffuses throughout the Co_3O_4 interstitial and interstitialcy spaces, it forms various intermediates such as $LiCo_2O_4$[8,9] and $Li_2Co_2O_4$.[7] An example of the intermediate found in the in-situ data is shown in Figure 5.

When the *d*-spacing of the 111 plane of Co_3O_4 ($Fd\bar{3}m$) lattice is plotted versus temperature, there is a linear increase along the *a*, *b*, and *c* axis, respectively, due to thermal expansion. As a result, the molar volume of the Co_3O_4 ($Fd\bar{3}m$) lattice is increased. Therefore, both the occupied and unoccupied tetrahedral as well as octahedral sites are expanded in the lattice. This molar volume increase promotes the reaction of molten Li_2CO_3 and the solid Co_3O_4 at the solid−liquid interface. Hence, the new structure is nucleated on the surface where the diffusion process precedes at a faster rate. As well, the reaction rate is accelerated when a liquid phase exists simultaneously.

The Co_3O_4 lattice increases isotropically until the temperature reaches 1000 K, where it begins to experience anisotropic growth due to the transformation from a cubic symmetry to rhombohedra symmetry as shown in Figure 7. Thus, the interconversion between the $Fd\bar{3}m$ symmetry of Co_3O_4 to $R\bar{3}m$ symmetry of $LiCoO_2$ is an allowed non-isomorphic transition. To compare the unit cells, both the 227 and 166 space groups were converted to their perspective primitive unit cells. **Note:** cubic crystals may be considered as a special cases of rhombohedral symmetry with the *P*, *I*, and *F* cells having primitive rhombohedral cells with 90°, 109.7°, and 60°, respectively.[26] The following transformation was used to convert the high symmetry $Fd\bar{3}m$ (227) to a primitive cubic cell: (0, 1/2, 1/2/1/2, 0, 1/2/1/2, 1/2, 0). As well, the following allowed isomorphic subgroup to group transformation used to convert $Fd\bar{3}m$ to $R\bar{3}m$: (−1/2a + 1/2b, −1/2b + 1/2c, a + b + c). The high symmetry $Li_2Co_2O_4$ cubic structure can transform to the low symmetry $R\bar{3}m$ structure with the following Wycoff splitting: Li^+ ion in the (227) 16c to (166) 3a, Co^{3+} ion in the (227) 16d to (166) 3b, and O^{2-} in the (227) 32e to the (166) 6c.

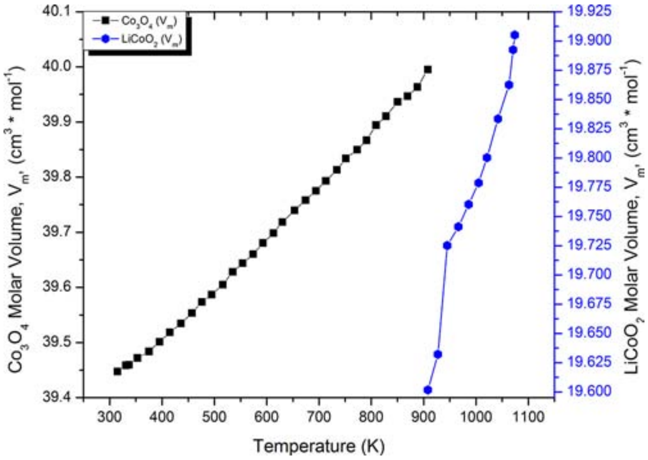

Figure 7. The plot of the molar volume vs temperature for Co_3O_4 and $LiCoO_2$.

It is our speculation that following transformation occurs at the oxygen-rich cubic lattice surface of the Co_3O_4. While the 16d octahedral sites are occupied by Co^{3+} ion and the 32e sites are occupied by O^{2-} ions, Li ions enter into the unoccupied 16c octahedral sites of the cubic Co_3O_4 lattice. This configuration describes the proposed $Li_2Co_2O_4$ $Fd\bar{3}m$ intermediate species that is shown in Figure 6. This intermediate species has an intergroup relationship with the original cubic spinel lattice $Fd\bar{3}m$ (227). As a result, the Co_3O_4 lattice is reduced along the *a*-axis, expanded along the *c*-axis, as well as the angle γ is increased from 90° to 120°.

Note: The Li^+ ions are known to migrate and occupy both the tetrahedral and octahedral sites giving rise to the spinel-type $Li_xCo_2O_4$ phase, where the Li^+ ion content is $x < 0.4$.[3,7−10,27,28] In this intermediate phase, only the intensities of the cubic spinel phase are reduced due to the displacement of the Co^{2+} with Li^+ within the 111 plane, while the intensities of the rhombohedral phase increase as shown in Figure 8. The trivalent cobalt ions have a predominant tendency to occupy octahedral sites in the lattice due to its low-spin state, which prevents migration to any tetrahedral sites. The growth along the *c*-axis is due to the horizontal or perpendicular alignment to the *c*-axis of trivalent cobalt ion in the octahedral sites. This is demonstrated by the increase in the intensity of the 003 peak of the rhombohedral phase located ~7.47 2θ and the decrease of the 111 peak of the spinel phase as shown in Figure 8.

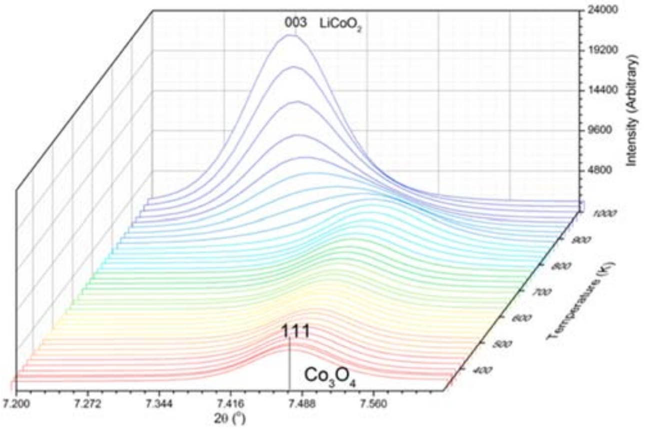

Figure 8. The reduction in intensity of the 111 peak of Co_3O_4 and the growth of the 003 of $LiCoO_2$.

Eventually, the pure spinel phase of the Co_3O_4 transforms into a lithiated spinel-type $Li_xCo_2O_4$ before rearranging into the rhombohedral phase of $LiCoO_2$, where $a = b \neq c$. Diffusion is believed to follow both interstitial and interstitialcy mechanisms.[29]

The higher intensity ratio of the (003) and (104) diffraction peaks, the clear splitting of the (006)/(102), as well as (108)/(110) diffraction peaks indicate excellent rhombohedral layered structure of the $LiCoO_2$ cathode by scan 41 (1074 K).[30−32] The integrated intensity ratio of (003) and (104) peaks (I_{003}/I_{104}) has been considered as one of the indicators to measure the degree of cation mixing.[33,34] This is because migration of Co ions from the octahedral (3a) site to Li (3b) site (and vice versa) is reported to weaken the intensity of (003) line. While such migrations do not alter the (104) peak intensity, the ratio is decreased with increased cation mixing. Typically, when the ratio (I_{003}/I_{104}) is less than 1.2, such as the case of several rhombohedral layered oxide cathodes, the reversible capacity has been reported to decrease. Several researchers have observed that when the intensity ratios was below 1.0 the rhombohedral layered oxide cathodes were electrochemically inactive.

Additionally, the *R* factor (defined by intensity ratio of $I_{006}/(I_{101} + I_{012})$ is considered to be another indicator of the rhombohedral ordering of the pristine cathode materials. Clear splitting of the (006/012) peaks indicates better rhombohedral ordering.[35] As well, the XRD peaks at (003) and (104), (101), (012), and (006) were intergrated using Bruker TOPAS software. The integrated intensities yielded the lattice parameters: *a*, *c*, *c*/*a* ratio, volumes, I_{003}/I_{104}, and *R*-factor were calculated to be 2.8355 Å, 14.2484 Å, 5.0250, 99.2175 Å^3, 1.5836, and 0.5744, respectively. The integrated intensity with the clear splitting of the peaks indicate reasonably good rhombohedral ordering in the pristined $LiCoO_2$ powders. A high intensity ratio of the I_{003}/I_{104} is a potential indication of desirable electrochemical properties.[36]

The rhombohedral ordering properties are very sensitive to the stoichiometry of the layered cathode oxides. The sensitivity is easily observed in the intergrated intensities and splitting of the (006), (012), and (101) reflections. For the stoichiometric $LiCoO_2$ compound, $R = ((I_{006} + I_{(012)})/I_{(101)} = 0.5744$.[37,38] The ratio *R* is 0.5744 for the $LiCoO_2$ sample in this study. Using the analytic approximation $R = 4/3\{(1.6 - x)/2x\}^2$ for $Li_xCo_{2-x}O_2$,[38,39] $x = 1.0622$. Thus, $x = 1.0622$ is a good indication that the $LiCoO_2$ sample is very close to stoichiometry.

Additionally, the X-ray experiments are in perfect agreement with the model-free kinetic studies that were performed over the same experimental conditions using a TA Q600 SDT thermal analysis instrument.

CONCLUSION

In conclusion, the solid-state synthesis of $LiCoO_2$ is a multistep process. The initial step involves the agglomeration of Li_2CO_3 particles followed by melting over a range of 700−900 K. Since the melting of Li_2CO_3 is not a thermodynamically favored process, this step is comparatively slower than the other two steps, as well as it has the highest activation energy (344 kJ/mol). The liquid Li_2CO_3 then forms a flux that reacts with Co_3O_4 particles at the liquid−solid interface, which involves the release CO_2 and diffusion of the Li^+ ions. As well, this endothermic process is clearly indicated in the plot of the E_α versus α. After Li ions diffuse into Co_3O_4 particles at the liquid−solid interface, structural rearrangement results in multiple intermediates before concluding at the electrochemically active $LiCoO_2$.

AUTHOR INFORMATION

Corresponding Author

*E-mail: edwin_walker@subr.edu.

Notes

The authors declare no competing financial interest.

ACKNOWLEDGMENTS

This research was made possible by a grant supplied by the National Science Foundation's Early CAREER program (Cooperative Agreement DMR-0449886), by the National Science Foundation's HBCU-RISE program (Cooperative Agreement HRD-1036588), and by a grant supplied by the U.S. Dept. of Education Title III Part B HBGI program (Grant No. P031B040030) at Southern University. Use of the Advanced Photon Source, an Office of Science User Facility operated for the U.S. Department of Energy (DOE) Office of Science by Argonned National Laboratory, was supported by the U.S. DOE under Contract No. DE-AC02-06CH11357. We would like to thank Drs. John Corbett, Weihua Wang, Catherine Page, David Johnson, and Les Butler for all the helpful discussions. As well, we would like to thank Dr. John Okasinski for all of the help at the Beamline.

REFERENCES

(1) Choi, K. Y.; Kim, K. D.; Yang, J. W. *J. Mater. Process. Technol.* **2006**, *171* (1), 118−124.

(2) Megahed, S.; Ebner, W. *J. Power Sources* **1995**, *54* (1), 155−162.

(3) Mizushima, K.; Jones, P. C.; Wiseman, P. J.; Goodenough, J. B. *Mater. Res. Bull.* **1980**, *15* (6), 783−789.

(4) Ohzuku, T.; Ueda, A. *J. Electrochem. Soc.* **1994**, *141* (11), 2972−2977.

(5) Reimers, J. N.; Dahn, J. R. *J. Electrochem. Soc.* **1992**, *139*, 2091.

(6) Tarascon, J. M.; Armand, M. *Nature* **2001**, *414* (6861), 359−367.

(7) Shao-Horn, Y.; Hackney, S. A.; Kahaian, A. J.; Thackeray, M. M. *J. Solid State Chem.* **2002**, *168* (1), 60−68.

(8) Meza, E.; Alburquenque, D.; Ortiz, J.; Gautier, J.-L. *J. Chil. Chem. Soc.* **2008**, *53* (2), 1494−1497.

(9) Appandairajan, N. K.; Viswanathan, B.; Gopalakrishnan, J. *J. Solid State Chem.* **1981**, *40* (1), 117−121.

(10) Shao-Horn, Y.; Levasseur, S.; Weill, F.; Delmas, C. *J. Electrochem. Soc.* **2003**, *150* (3), A366−A373.

(11) Lu, C.-H.; Yeh, P.-Y.; Hsu, W.-T. *J. Alloys Compd.* **2009**, *476* (1−2), 749−754.

(12) Vyazovkin, S.; Wight, C. A. *Annu. Rev. Phys. Chem.* **1997**, *48* (1), 125−149.

(13) Vyazovkin, S. V.; Lesnikovich, A. I. *Thermochim. Acta* **1990**, *165* (2), 273−280.

(14) Vyazovkin, S. V.; Goryachko, V. I.; Lesnikovich, A. I. *Thermochim. Acta* **1992**, *197* (1), 41−51.

(15) Vyazovkin, S. *Thermochim. Acta* **1994**, *236*, 1−13.

(16) Vyazovkin, S.; Linert, W. *Int. J. Chem. Kinet.* **1995**, *27* (1), 73−84.

(17) Vyazovkin, S. *Thermochim. Acta* **1993**, *223*, 201−206.

(18) Flynn, J. H.; Wall, L. A. *J. Res. Natl. Bureau Stand., A. Phys. Chem.* **1966**, *70*, 487−523.

(19) Friedman, H. L. *J. Polym. Sci. Part C: Polym. Symp.* **1964**, *6* (1), 183−195.

(20) Ozawa, T. *Bull. Chem. Soc. Jpn.* **1965**, *38*, 1881−1886.

(21) Burukhin, A.; Brylev, O.; Hany, P.; Churagulov, B. R. *Solid State Ionics* **2002**, *151* (1−4), 259−263.

(22) Chupas, P. J.; Chapman, K. W.; Kurtz, C.; Hanson, J. C.; Lee, P. L.; Grey, C. P. *J. Appl. Crystallogr.* **2008**, *41* (4), 822−824.

(23) Friedman, H. L. *J. Polym. Sci. Part B: Polym. Lett.* **1969**, *7* (1), 41−46.

(24) Vyazovkin, S. *J. Comput. Chem.* **2001**, *22* (2), 178−183.

(25) Ktalkherman, M. G. E.; Pozdnyakov, V. A. *Theor. Found. Chem. Eng.* **2008**, *43* (1), 93−98.

(26) O'Keeffe, M.; Hyde, B. G. *Crystal Structures*; Mineralogical Society of America: Chelsea, MI, 1996; Vol. *1*, p 453.

(27) Antolini, E. *Solid State Ionics* **2004**, *170* (3−4), 159−171.

(28) Levasseur, S.; Ménétrier, M.; Shao-Horn, Y.; Gautier, L.; Audemer, A.; Demazeau, G.; Largeteau, A.; Delmas, C. *Chem. Mater.* **2002**, *15* (1), 348−354.

(29) Lu, C.-H.; Wei-Cheng, L. *J. Mater. Chem.* **2000**, *10* (6), 1403−1407.

(30) Hwang, B. J.; Santhanam, R.; Chen, C. H. *J. Power Sources* **2003**, *114*, 244.

(31) Majumder, S. B.; Nieto, S.; Katiyar, R. S. *J. Power Sources* **2006**, *154*, 262.

(32) Periasamy, P.; Kim, H.-S.; Na, S. H.; Moon, S. I.; Lee, J. C. *J. Power Sources* **2004**, *132*, 213.

(33) Li, D.; Sasaki, Y.; Kobayakawa, K.; Sato, Y. *J. Power Sources* **2006**, *157*, 488.

(34) Ohzuhu, T.; Ueda, A.; Nagayama, M.; Iwakoshi, Y.; Konomri, H. *Electrochim. Acta* **1993**, *38*, 1159.

(35) Goa, Y.; Yakovleva, M. V.; Ebner, W. B. *Electrochem. Solid State Lett.* **1998**, *1*, 117.

(36) Sivaprakash, S.; Majumder, S. B.; Nieto, S.; Katiyar, R. S. *J. Power Sources* **2007**, *170*, 433−440.

(37) Reimers, J. N. D.; Dahn, J. R.; Greedan, J. E.; Stager, C. V.; Lui, G.; Davidson, I.; von Sacken, U. *J. Solid State Chem.* **1993**, *102*, 542.

(38) Wang, M.; Navrotsky, A. *Solid State Ionics* **2004**, *166*, 167−173.

(39) Dahn, J. R.; von Sacken, U.; Michal, C. A. *Solid State Ionics* **1990**, *44*, 87.